Research Article | Vol. 27, No. 23 / 11 November 2019 / Optics Express 33789
Optics EXPRESS

Experimental demonstration of 111.1-Gb/s net information rate using IM/DD probabilistically shaped orthogonal chirp-division multiplexing with a 10-GHz-class modulator

ZHOUYI HU,[1] YINGJIE SHAO,[1] XING OUYANG,[2] YEYU TONG,[3] JIAN ZHAO,[4] HON KI TSANG,[3] PAUL D. TOWNSEND,[2] AND CHUN-KIT CHAN[1,*]

[1] *Department of Information Engineering, The Chinese University of Hong Kong, Hong Kong, China*
[2] *Tyndall National Institute and University College Cork, Cork, Ireland*
[3] *Department of Electronic Engineering, The Chinese University of Hong Kong, Hong Kong, China*
[4] *South China University of Technology, Guangzhou, China*
[*] *ckchan@ie.cuhk.edu.hk*

Abstract: We propose probabilistically shaped quadrature amplitude modulation (PS-QAM) formats to maximize the capacity in fiber transmission systems using orthogonal chirp-division multiplexing (OCDM). OCDM possesses the property of chirp spread spectrum (CSS), leading to improved resilience to system impairments. We further investigate the recently proposed robust channel estimator based on pulse compression and noise rejection and experimentally demonstrate its feasibility in an intensity-modulated/direction-detection (IM/DD) OCDM system. By applying the proposed PS-QAM based OCDM to an IM/DD optical system, a net information rate of 111.1 Gb/s has been successfully achieved using a 10-GHz class Mach–Zehnder modulator (MZM) and has also shown improved performance compared to the conventional PS-QAM based orthogonal frequency-division multiplexing (OFDM) systems. Moreover, due to the superior characteristics of OCDM, there is no need for additional feedback to obtain the prior knowledge of channel state information in the proposed system, leading to reduced complexity and cost.

1. Introduction

Owing to the ever-growing demand for capacity, various signal processing techniques, including high-order modulation formats and sophisticated digital signal processing (DSP) algorithms [1–3] have been reported for high-speed fiber-optic communication systems. The recently proposed orthogonal chirp-division multiplexing (OCDM) technology is an attractive solution, due to its improved resilience to system impairments [4–6] compared to the conventional orthogonal frequency-division multiplexing (OFDM). However, as a chirp spread spectrum (CSS) technique, OCDM intrinsically spreads information over the spectrum. As a result, adaptive loading, which has been widely used in OFDM, cannot be applied to OCDM systems to maximize the capacity.

On the other hand, probabilistically shaped (PS) quadrature amplitude modulation (QAM) has been demonstrated to provide near-optimal energy efficiency, and can thus approach the Shannon limit in an additive white Gaussian noise (AWGN) channel [7,8]. Although combining adaptive loading with PS can achieve the optimal performance [9,10], applying PS with different distribution to each subcarrier of an OFDM signal results in extremely high complexity. The OFDM system combining pre-equalization and uniform PS-QAM formats was thus proposed to achieve a good compromise between performance and complexity [11]. However, in both cases, the additional feedback link was necessary for the prior knowledge of channel state information (CSI). Alternatively, the CSI-free precoded OFDM with uniform PS was recently reported to achieve the similar performance [12–14]. However, the additional precoding process still results

#377471 https://doi.org/10.1364/OE.27.033789
Journal © 2019 Received 9 Sep 2019; revised 25 Oct 2019; accepted 26 Oct 2019; published 4 Nov 2019

Optics EXPRESS

in increased computational complexity when the number of subcarrier is large. Fortunately, OCDM can spread the system impairments over the spectrum without requiring CSI. Moreover, due to the high compatibility of OCDM to OFDM, an OCDM transmitter only needs two additional diagonal matrices [4] compared to OFDM, leading to very low increase in complexity.

In this paper, we propose, for the first time, a PS-QAM based OCDM system in order to achieve the maximal capacity of an optical system. We further investigate a robust channel estimation scheme based on pulse compression and noise rejection (PCNR) [15], which shows improved performance in an intensity-modulated/direct-detection (IM/DD) OCDM system, compared to the conventional intra-symbol frequency-domain averaging (ISFA) based method [16]. With the help of PS and PCNR, we successfully achieve a net information rate of 111.1 Gb/s using PS-256-QAM based OCDM in a 2.5-km IM/DD fiber-optic system under only 10-GHz 6-dB system bandwidth, after considering the forward error correction (FEC) and other overhead (OH), such as CP and pilots for channel estimation. In the verified IM/DD system, the additional feedback link for the prior knowledge of CSI is also omitted due to the superior characteristics of OCDM.

2. Principle

2.1. OCDM with PCNR for IM/DD systems

As illustrated in Fig. 1(a), OCDM spreads information over the spectrum by modulating the quadratic exponential waveforms which are essentially linear frequency modulated signals or termed as chirps. The chirps are different from the linear exponential waveforms used in OFDM (see Fig. 1(b)). Due to the property of CSS, OCDM can spread information and equalize the degradation over spectrum, leading to improved performance [4–6]. The recently proposed inverse discrete Fresnel transform (IDFnT) can efficiently generate a discrete-time OCDM signal [4], as

$$S(n) = \mathcal{F}_{\Psi}^{-1}\{x(k)\} = e^{j\frac{\pi}{4}} \sum_{k=0}^{N-1} x(k) \times \begin{cases} e^{-j\frac{\pi}{N}(n-k)^2} & N \equiv 0 \pmod 2 \\ e^{-j\frac{\pi}{N}\left(n-k+\frac{1}{2}\right)^2} & N \equiv 1 \pmod 2 \end{cases} \tag{1}$$

where $\mathcal{F}_{\Psi}^{-1}\{\cdot\}$ denotes the operation of IDFnT, $x(k)$ is the symbol modulating the k-th chirp, and $S(n)$ is the n-th time sample of an OCDM symbol.

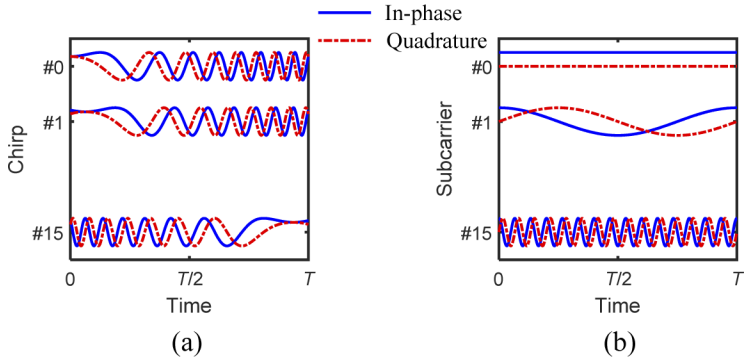

Fig. 1. Illustration of the waveforms in (a) OCDM and (b) OFDM.

Since each of the chirps occupies the whole bandwidth of the signal, a channel estimator, termed as PCNR, was recently proposed to efficiently utilize the advantages of the chirped signals [15]. Figure 2 shows the block diagram of PCNR, where the operations highlighted in red dash

Optics EXPRESS

line are only required for an IM/DD OCDM system. The estimated impulse response function of the system is obtained by the pulse compression of the chirp, as

$$\psi_k^*(n) = \mathcal{F}_\Psi^{-1}\{\delta(n-k)\} \tag{2}$$

$$\begin{aligned}\hat{h}_\Psi(m) &= \mathcal{F}_\Psi\{h(n) \otimes \psi_k^*(n) + v(n)\} \\ &= h(m) \otimes \delta(m-k) + v_\Psi(m) \\ &= h(m-k) + v_\Psi(m)\end{aligned} \tag{3}$$

where $\delta(k)$ denotes the Kronecker delta function, $\otimes$ is the circular convolution operator, $v(n)$ is AWGN, and $h(m)$ is the channel impulse response. Note that the chirped pilot $\psi_k^*(n)$ can be readily chosen from an IDFnT matrix, i.e., the k-th column of the IDFnT matrix. Another advantage of this channel estimator is its superior performance realized by a simple gate function $\Pi_G(m)$ with a width of L_Π to reject the excessive noise. The resultant channel frequency response (CFR) after noise rejection is thus given by

$$\hat{H}_\Pi(m) = \mathcal{F}_\Omega\{\Pi_G(m)\hat{h}_\Psi(m)\} \tag{4}$$

where $\mathcal{F}_\Omega$ denotes the operation of DFT. PCNR has been shown to offer improved performance in coherent-OCDM systems, compared to the widely adopted ISFA estimator [16]. In this work, we implement, for the first time, PCNR in a high-speed IM/DD OCDM system.

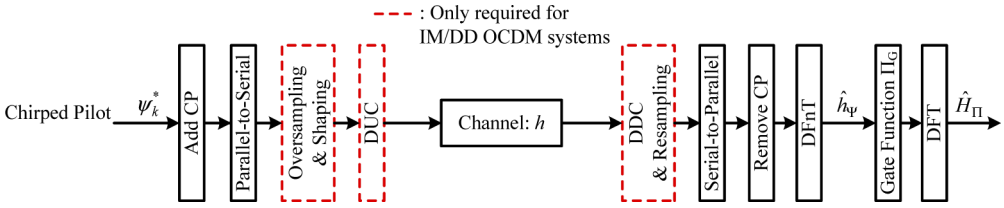

Fig. 2. Block diagram of PCNR for IM/DD OCDM systems (DUC: digital up-conversion; DDC: digital down-conversion).

Without loss of generality, $\psi_0^*(n)$ is chosen as chirped pilot, as presented in Fig. 3. The

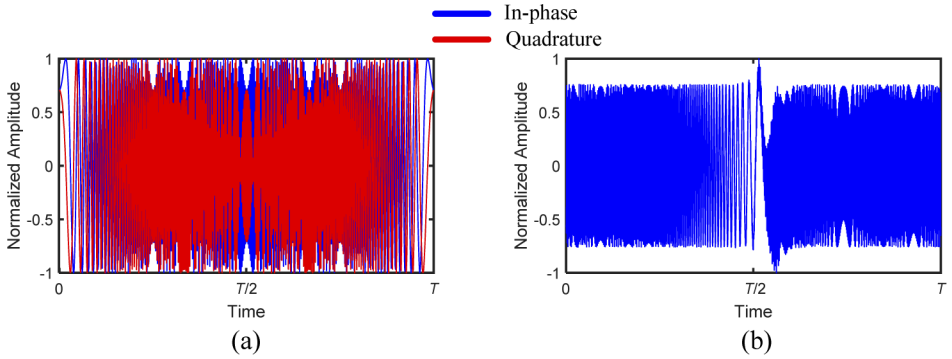

Fig. 3. Illustration of (a) the original complex-valued pilot signal, and (b) the up-converted real-valued pilot signal.

original chirped pilot for coherent optical communications [15] is shown in Fig. 3(a), which is complex-valued. To implement an IM/DD OCDM system [6], the complex-valued chirped pilot

Optics EXPRESS

should be first up-converted to the passband via digital up-conversion (DUC) at the transmitter side. We can then obtain a real-valued double-sideband pilot signal for transmission, as

$$\Phi_0^*(t) = \mathrm{Re}\{\psi_0^*(t)e^{j2\pi f_c t}\} \tag{5}$$

where $\psi_0^*(t)$ is the time-domain chirped pilot after oversampling and pulse shaping, f_c is the carrier frequency for DUC. It should be noted that f_c must be large enough to ensure a guard band for anti-aliasing. Figure 3(b) shows the converted pilot $\Phi_0^*(n)$ in Eq. (5) for IM/DD OCDM, where f_c=11.9325 GHz, and the guard band was set to 0.12 GHz, corresponding to the experiment presented later in the section 3.

2.2. PS-QAM formats based OCDM

As aforementioned, the property of CSS in OCDM provides improved resilience to system impairments, compared to OFDM. However, CSS prevents adaptive loading for maximizing the system capacity in an OCDM system. Nonetheless, the ability to spread degradation over spectrum in OCDM systems can be utilized to maximize the coding gain from the uniform PS and thus approach the system capacity limit. This shares the similar mechanism as precoded OFDM and pre-equalized OFDM [11–14]. However, it should be noted that OCDM does not require additional complex precoding nor a feedback link, indicating its lower complexity in terms of both DSP and devices. For instance, compared to the recently proposed orthogonal circulant matrix transform (OCT) based precoding scheme [13,14], the number of required additional complex-valued multiplications is reduced from N/subcarrier in precoded-OFDM transmitter to only 2/chirp in OCDM transmitter [4], where N is the number of subcarriers/chirps.

Figure 4 shows the block diagram of PS-QAM mapping [7] before performing OCDM modulation, where the information rate at each step is also presented. It can be seen that the probability distribution of amplitudes is jointly determined by the employed distribution matcher (DM) and the desired entropy rate. In this work, Maxwell-Boltzmann (MB) distribution realized by constant composition distribution matching (CCDM) is adopted for its superior performance in the AWGN channel [7,17]. On the other hand, we can see from the figure that the achieved net information rate is $2(\beta + \gamma)$ bits/PS-QAM symbol, which is related to both the entropy rate and the coding rate of FEC. After ignoring entropy loss from DM, β is given by

$$\beta = \mathbb{H}(X_{\mathrm{PAM}}) - 1 \tag{6}$$

where $\mathbb{H}(X_{\mathrm{PAM}})$ denotes the entropy rate of PS-pulse amplitude modulation (PS-PAM) symbols. Since the sign bit carries both the FEC OH, i.e., parity check bit, and the information content (γ), we have

$$\gamma = m_{\mathrm{PAM}}(R_c - 1) + 1 \tag{7}$$

where R_c denotes the FEC coding rate, and m_{PAM} is the information rate of the adopted PAM format for mapping (e.g., m_{PAM}=3 for PAM-8). Note that in order to ensure $\gamma \geq 0$, we have

$$R_c \geq \frac{m_{\mathrm{PAM}} - 1}{m_{\mathrm{PAM}}} \tag{8}$$

which is the code rate constraint in PS-based systems [18].

For the sake of simplicity, the FEC encoding/decoding was omitted in this work. Alternatively, the normalized generalized mutual information (NGMI) was adopted to evaluate the performance, which has been widely used as a precise prediction method for the post-FEC BER [18–21].

Optics EXPRESS

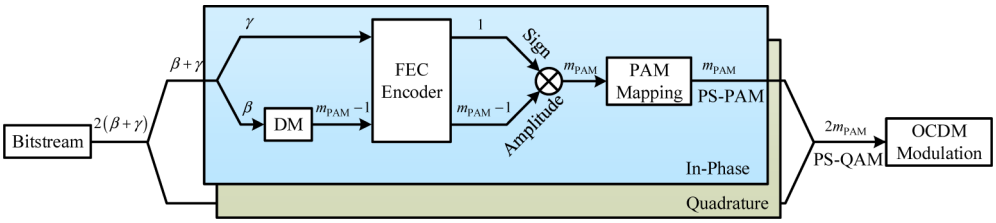

Fig. 4. Block diagram of PS-QAM generator for the proposed PS-QAM based OCDM system.

NGMI of PS-QAM can be derived from GMI, as

$$GMI_{\mathrm{QAM}} \approx 2\mathbb{H}(X_{\mathrm{PAM}}) + \frac{2}{N}\sum_{l=1}^{L}\sum_{i=1}^{m_{\mathrm{PAM}}}\log_2\frac{\sum_{x\in\chi\_b_{l,i}} \mathrm{q}(y_l|x)\mathrm{P}(x)}{\sum_{x\in\chi}\mathrm{q}(y_l|x)\mathrm{P}(x)} \tag{9}$$

$$NGMI_{\mathrm{QAM}} = 1 - \frac{2\mathbb{H}(X_{\mathrm{PAM}}) - GMI_{\mathrm{QAM}}}{2m_{\mathrm{PAM}}} \tag{10}$$

where L is the number of received symbols for estimation, χ is the set of PAM symbols, $b_{l,i}$ denotes the i-th bit of the l-th transmitted symbol, the function $\mathrm{q}(y|x)$ returns the probability density of the received symbol y given the transmitted symbol x in the memoryless AWGN channel, and $\mathrm{P}(x)$ is the probability mass function determined by DM [21].

3. Experimental setup

Figure 5 shows the experimental setup and DSP of the proposed PS-QAM based IM/DD OCDM system with PCNR. The bitstream was first mapped into PS-QAM symbols via the architecture shown in Fig. 4. An 864-point IDFnT was then employed to generate a complex-valued OCDM signal. The CP, with a length of 1/16 of one OCDM symbol, was added as guard interval. A single chirped pilot symbol was inserted before every 200 payload symbols (0.5% OH). After parallel-to-serial conversion, we applied oversampling (64/27 times), Nyquist shaping and DUC to the complex-valued baseband OCDM signal in order to obtain a real-valued OCDM signal for our IM/DD system. The analog signal was generated by an arbitrary waveform generator (AWG, Keysight AWG M8195A) working at 56 GSa/s. Therefore, the complex baseband signal has a bandwidth 23.625 (=56 × 27/64) GHz. Since the guard band was set to 0.12 GHz, the required f_c as given in Eq. (5) was 11.9325 (=23.625/2 + 0.12) GHz. A laser diode (LD) working at ~1550 nm and a 10-GHz-class commercial Mach-Zehnder modulator (MZM, IOAP-MOD9140) were then used for external modulation. The launched power of the modulated optical signal was 6.3 dBm, before being fed into a 2.5-km SSMF link.

At the receiver, a variable optical attenuator (VOA) was used to vary the received optical power (ROP). Finally, the signal was captured by a 160-GSa/s digital storage oscilloscope (DSO, Teledyne Lecroy LabMaster 10-25Zi) after DD by a 31-GHz photodetector (PD, MPRV1331A). To obtain an accurate CFR, the received chirped pilot was sent to a PCNR module, as shown in Fig. 5. On the other hand, the offline DSP for the payload symbols included digital down-conversion (DDC), resampling, serial-to-parallel conversion, CP removal, DFT, phase rotation [4], single-tap equalization based on the CFR from PCNR, and inverse DFT (IDFT) to recover the PS-QAM symbols. Finally, NGMI given in Eqs. (9)–(10) was utilized to evaluate the quality of the received PS-QAM symbols.

In this work, we have also investigated OFDM based systems to verify the performance of the proposed OCDM based system. For a fair comparison, the OFDM signal had 2048 subcarriers, among which 864 subcarriers at the positive frequency were effectively modulated. Except for

Optics EXPRESS

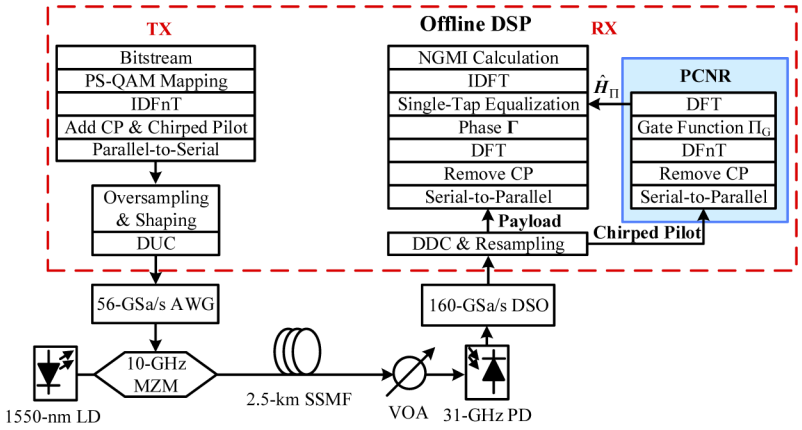

Fig. 5. Block diagram of the proposed PS-QAM based IM/DD OCDM system with PCNR.

the unfilled DC component, the modulated subcarriers were selected around zero frequency. Hermitian symmetry was then applied to the negative frequency to generate a real-valued OFDM signal.

4. Experimental results

4.1. OCDM with PCNR in IM/DD systems

The received real-valued chirped pilot signal is presented in Fig. 6(a). The attenuation at the high frequencies is much higher than that at the low frequencies due to severe channel fading. Meanwhile, the influence of AWGN can be observed in Fig. 6(b), showing the impulse response before noise rejection. Since CSI is determined by the impulse response, we can readily eliminate the out-of-band noise by a gate function, as shown in Eq. (4). The estimated CFRs without and with noise rejection are presented in Fig. 6(c) and Fig. 6(d), respectively. Thanks to the

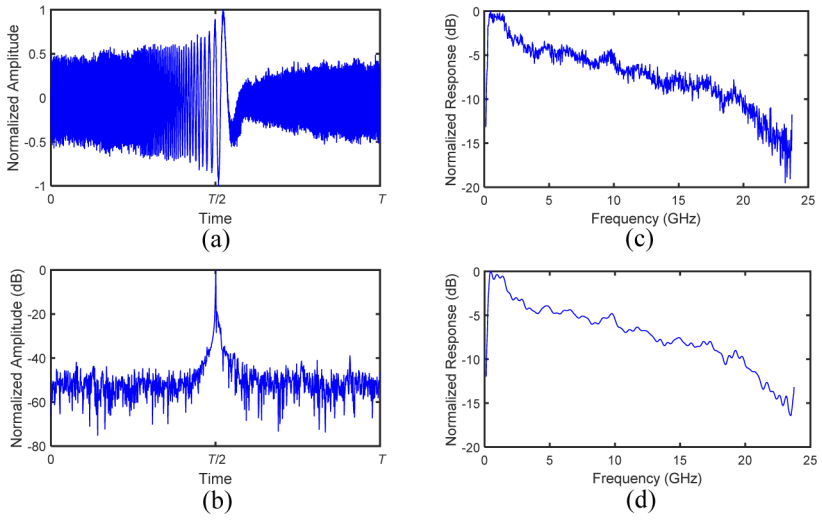

Fig. 6. (a) The received chirped pilot signal; (b) Impulse response before noise rejection; (c) The estimated CFR without noise rejection; (d) The estimated CFR with noise rejection.

Optics EXPRESS

employed gate function, the major impact of AWGN can be significantly mitigated. We can see from the CFR that the 3-dB bandwidth of our IM/DD system is only about 2 GHz, which can be attributed to the cascaded frequency roll-off effect caused by all the involved components/devices. Meanwhile, the 6-dB bandwidth is about 10 GHz.

We then verified the performance of PCNR in the proposed IM/DD fiber-optic system by comparing the OCDM signal with PCNR, the OCDM signal with ISFA and the OFDM signal with ISFA, where uniform-32-QAM is used for modulation, and the ROP is fixed at – 4 dBm. Note that PCNR was proposed for OCDM, and cannot be applied to OFDM directly. The size of the averaging window D_w in the ISFA [16] was optimized in Fig. 7(a), which presents the pre-FEC BER as a function of D_w. Results are also compared with the PCNR based OCDM signal using the optimal gate window. We can see from the figure that the OCDM signal with PCNR always outperforms the case with ISFA, which can be attributed to its more accurate channel estimation compared to the ISFA based method. This can also be verified by their signal-to-noise ratio (SNR) profiles depicted in Fig. 7(b), where ~0.5-dB improvement is achieved by PCNR. On the other hand, in contrast to OFDM, OCDM spreads the impairments over the spectrum, and can thus realize the CSI-free pre-equalization. Note that both the improvements from the PCNR and the CSI-free pre-equalization can help maximize the system capacity of the proposed scheme via the advanced PS-QAM formats.

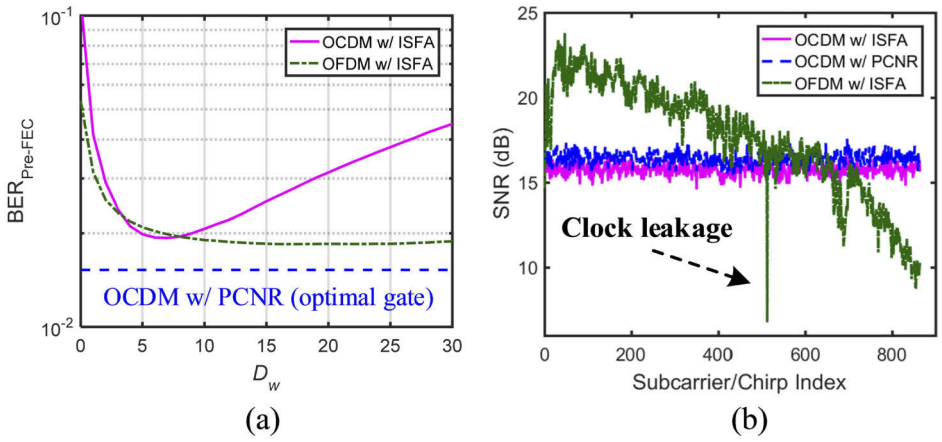

Fig. 7. (a) Pre-FEC BER versus the size of averaging window in the ISFA, where the PCNR is also attached for comparison. (b) The measured SNR profiles of different signals.

4.2. PS-QAM based OCDM with PCNR

Figure 8(a) presents NGMI versus the ROP for different signals, including OCDM with only ISFA, OCDM with only PCNR, OCDM with both PCNR and PS-QAM, the conventional OFDM with only ISFA, and the conventional OFDM with both ISFA and PS-QAM. PS-64-QAM with 5-bits/symbol entropy rate (corresponding to uniform-32-QAM) was used for PS based systems. The improved performance of PCNR has also been verified at all ROP values. Moreover, we can see from the figure that the employment of PS-QAM significantly improves the NGMI for both OCDM and OFDM signals. Although OCDM with PS-QAM shows relatively poor performance at low ROP region, it can outperform the OFDM signal with PS-QAM when ROP is larger than – 6 dBm. Especially when ROP is – 4 dBm, with the help of PCNR and the CSS property of OCDM, the proposed PS-QAM scheme can improve the NGMI from 0.9618 to 0.9961.

We then investigated the upper capacity limits of the OCDM and the OFDM based systems, respectively. As shown in Fig. 8(b), when PS-64-QAM symbols are used for modulation,

Optics EXPRESS

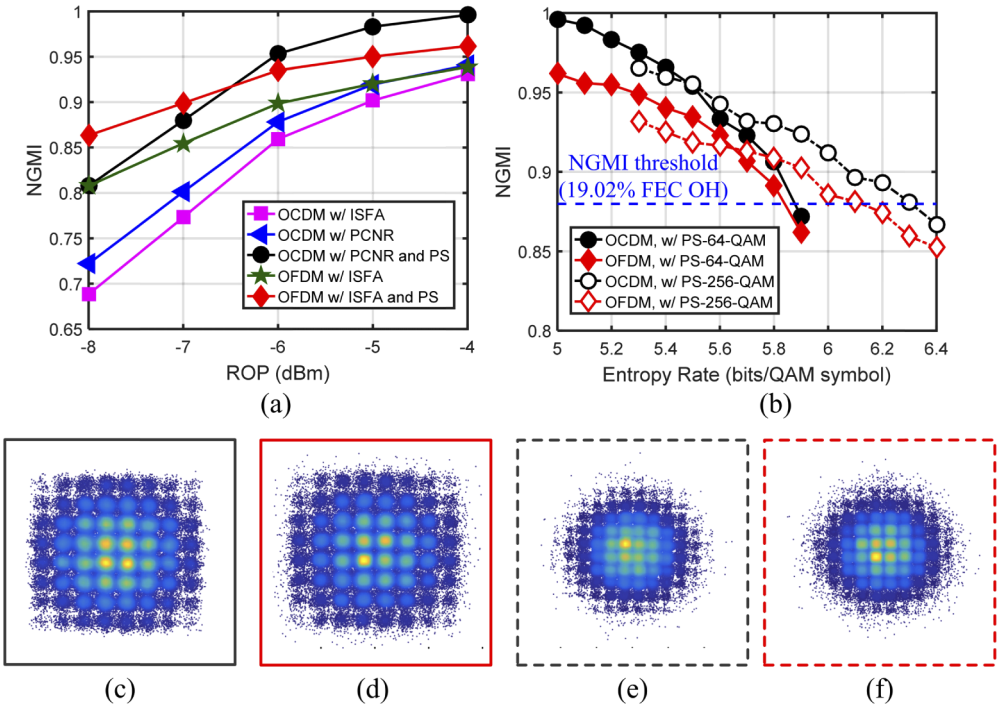

Fig. 8. Calculated NGMI versus (a) ROP (5-bits/symbol entropy rate) and (b) entropy rate (ROP=−4 dBm). Received constellation diagrams of PS-64-QAM in (c) OCDM signal and (d) OFDM signal; Received constellation diagrams of PS-256-QAM in (e) OCDM signal and (f) OFDM signal. (Entropy rates are all 5.3 bits/symbol)

the NGMI decreases rapidly as the entropy rate approaches 6 bits/symbol (corresponding to uniform-64-QAM). Therefore, we applied PS-256-QAM to our system at the region of high entropy rate. The received constellation diagrams of these two shaping schemes applied to OCDM and OFDM signals are presented in Fig. 8(c-f). We can see that the received symbols in OFDM based systems are more scattered than that in OCDM based systems, especially for the outer symbols. As the results shown in Fig. 8(b), in comparison with the PS-QAM based OFDM system, the proposed PS-QAM based OCDM system can improve the maximum entropy rate from 6.1 bits/symbol to 6.3 bits/symbol at the NGMI threshold of 0.8798. As demonstrated in [21], this NGMI threshold corresponds to the FEC with a code rate of 0.8402 (i.e., 19.02% OH), which consists of a spatially-coupled low-density parity-check (SC-LDPC) code of code rate 0.8469 and an outer hard-decision BCH (8191, 8126, 5) code. We assume that the same FEC code was used in this work. For PS-256-QAM with this FEC, we have γ=0.3608, according to Eq. (7). Considering CP, FEC, pilot and other OH [18], a net information rate can be calculated by

$$R_{net} = R_{AWG}/Ratio_{oversampling} \times 2(\beta + \gamma) \times \frac{1}{1 + OH_{CP}} \times \frac{1}{1 + OH_{pilot}}, \tag{11}$$

where β is obtained by Eq. (6). Therefore, in this work, a net information rate of 111.1 Gb/s (= 56 G × 27/64 × (6.3 − 2 + 0.3608 × 2) × 16/17 × 200/201) has been successfully achieved by the proposed IM/DD fiber-optic system.

It should be noted that since OCDM, as well as the other precoded OFDM schemes, spreads the impairments over the entire bandwidth, the effective SNR of OCDM signals is the harmonics mean of per-subcarrier SNRs. On the other hand, the effective SNR of OFDM signals is the

Optics EXPRESS

geometric mean of per-subcarrier SNRs [22,23]. As a result, OCDM has a lower capacity than OFDM unless the channel is flat. However, in practical applications, we can only approach the capacity limit of an OFDM system when we know the accurate CSI at the transmitter side, leading to increased system complexity as well as cost. Therefore, the proposed scheme can achieve a higher data rate than OFDM systems when the CSI cannot be obtained or utilized at the transmitter side, at the expense of a decrease in total channel capacity.

5. Summary

In this paper, we have proposed, for the first time, a PS-QAM based OCDM system with PCNR to maximize the system capacity. Due to the spread-spectrum property of OCDM, the proposed scheme has achieved the superior performance compared to the conventional PS-QAM based OFDM system. By avoiding the round-trip delay and the cost of a feedback link for the CSI estimation at the transmitter, the system complexity as well as the cost can be significantly reduced. A net information rate of 111.1 Gb/s has been experimentally demonstrated in a 2.5-km IM/DD fiber-optic system with a 10-GHz-class MZM, indicating its great potential in high-speed and short-reach applications, such as intra-datacenter connections.

Funding

Science Foundation Ireland (12/IA/1270, 12/RC/2276 P2); Science and Technology Planning Project of Guangdong Province (2019A050503003); Guangzhou Science and Technology Program key projects (201904010298).

Disclosures

The authors declare no conflicts of interest.

References

1. K. Zhong, X. Zhou, T. Gui, L. Tao, Y. Gao, W. Chen, J. Man, L. Zeng, A. Pak, T. Lau, and C. Lu, "Experimental Study of PAM-4, CAP-16, and DMT for 100 Gb/s Short Reach Optical Transmission Systems," Opt. Express **23**(2), 1176–1189 (2015).
2. Z. Li, M. S. Erkılınç, K. Shi, E. Sillekens, L. Galdino, T. Xu, B. C. Thomsen, P. Bayvel, and R. I. Killey, "Spectrally Efficient 168 Gb/s/λ WDM 64-QAM Single-Sideband Nyquist-Subcarrier Modulation with Kramers-Kronig Direct-Detection Receivers," J. Lightwave Technol. **36**(6), 1340–1346 (2018).
3. M. Mazur, A. Lorences-Riesgo, J. Schröder, P. A. Andrekson, and M. Karlsson, "10 Tb/s PM-64QAM Self-Homodyne Comb-Based Superchannel Transmission With 4% Shared Pilot Tone Overhead," J. Lightwave Technol. **36**(16), 3176–3184 (2018).
4. X. Ouyang and J. Zhao, "Orthogonal chirp division multiplexing," IEEE Trans. Commun. **64**(9), 3946–3957 (2016).
5. X. Ouyang and J. Zhao, "Orthogonal chirp division multiplexing for coherent optical fiber communications," J. Lightwave Technol. **34**(18), 4376–4386 (2016).
6. X. Ouyang, G. Talli, M. Power, and P. Townsend, "Orthogonal chirp-division multiplexing for IM/DD-based short-reach systems," Opt. Express **27**(16), 23620–23632 (2019).
7. F. Buchali, F. Steiner, G. Böcherer, L. Schmalen, P. Schulte, and W. Idler, "Rate Adaptation and Reach Increase by Probabilistically Shaped 64-QAM: An Experimental Demonstration," J. Lightwave Technol. **34**(7), 1599–1609 (2016).
8. G. Böcherer, F. Steiner, and P. Schulte, "Bandwidth Efficient and Rate-Matched Low-Density Parity-Check Coded Modulation," IEEE Trans. Commun. **63**(12), 4651–4665 (2015).
9. D. Che and W. Shieh, "Achievable Rate Comparison between Entropy and Bit Loading in a 100-Gb/s DM-DD DMT System," in *Optical Fiber Communication Conference* (Optical Society of America, March 2019), paper W1F.3.
10. X. Chen, S. Chandrasekhar, J. Cho, and P. Winzer, "Single-Wavelength and Single-Photodiode Entropy-Loaded 554-Gb/s Transmission over 22-km SMF," in *Optical Fiber Communication Conference* (Optical Society of America, March 2019), paper Th4B.5.
11. J. Shi, J. Zhang, N. Chi, Y. Cai, X. Li, Y. Zhang, Q. Zhang, and J. Yu, "Probabilistically Shaped 1024-QAM OFDM Transmission in an IM-DD System," in *Optical Fiber Communication Conference* (Optical Society of America, March 2018), paper W2A.44.

Optics EXPRESS

12. X. Chen, Y. Chen, M. Tang, H. Zhou, J. Cui, T. Tong, S. Fu, and D. Liu, "Uniform Entropy Loading for Precoded DMT Systems in Fading Optical Channel," in *Proc. Asia Communications and Photonics Conference*, Hangzhou, China, October 2018, pp. 1–3.
13. K. Wu, J. He, Z. Zhou, J. He, and J. Shi, "Probabilistic Amplitude Shaping for a 64-QAM OFDM W-Band RoF System," IEEE Photonics Technol. Lett. **31**(13), 1076–1079 (2019).
14. Y. Shao, Y. Hong, Z. Hu, and L. K. Chen, "Capacity Maximization of OWC Systems via Joint Precoding and Probabilistic Shaping," IEEE Photonics Technol. Lett. **31**(13), 1013–1016 (2019).
15. X. Ouyang, C. Antony, G. Talli, and P. Townsend, "Robust Channel Estimation for Coherent Optical Orthogonal Chirp-Division Multiplexing with Pulse Compression and Noise Rejection," J. Lightwave Technol. **36**(23), 5600–5610 (2018).
16. X. Liu and F. Buchali, "Intra-Symbol Frequency-Domain Averaging based Channel Estimation for Coherent Optical OFDM," Opt. Express **16**(26), 21944–21957 (2008).
17. P. Schulte and G. Böcherer, "Constant Composition Distribution Matching," IEEE Trans. Inf. Theory **62**(1), 430–434 (2016).
18. J. Cho, X. Chen, S. Chandrasekhar, and P. Winzer, "On Line Rates, Information Rates, and Spectral Efficiencies in Probabilistically Shaped QAM Systems," Opt. Express **26**(8), 9784–9791 (2018).
19. A. Alvarado, E. Agrell, D. Lavery, R. Maher, and P. Bayvel, "Replacing the Soft-Decision FEC Limit Paradigm in the Design of Optical Communication Systems," J. Lightwave Technol. **33**(20), 4338–4352 (2015).
20. J. Cho, L. Schmalen, and P. Winzer, "Normalized Generalized Mutual Information as a Forward Error Correction Threshold for Probabilistically Shaped QAM," in *Proc. Eur. Conf. Exhib. Opt. Commun.*, Gothenburg, Sweden, September 2017, Paper M.2.D.
21. S. L. I. Olsson, J. Cho, S. Chandrasekhar, X. Chen, P. Winzer, and S. Makovejs, "Probabilistically Shaped PDM 4096-QAM Transmission over up to 200 Km of Fiber Using Standard Intradyne Detection," Opt. Express **26**(4), 4522–4530 (2018).
22. M. Hua, B. Ren, M. Wang, J. Zou, C. Yang, and T. Liu, "Performance analysis of OFDMA and SC-FDMA multiple access techniques for next generation wireless communications," in *Proc. IEEE Veh. Technol. Conf.* (VTC Spring'13), Dresden, Germany, June 2013, pp. 1–4.
23. Y. Shao, Y. Hong, and L. K. Chen, "On CSI-free Linear Equalization for Optical Fast-OFDM over Visible Light Communications," in *Optical Fiber Communication Conference* (Optical Society of America, March 2018), paper M3 K.5.